Improved transient plane source measurements of layer–substrate structures via a semi-analytical temperature response model

Citation for the original published paper (version of record):
Zeng, Z., Müller, C., Gustavsson, J. et al (2026). Improved transient plane source measurements of layer–substrate structures via a
semi-analytical temperature response model. International Journal of Heat and Mass Transfer, 261.
http://dx.doi.org/10.1016/j.ijheatmasstransfer.2026.128581

International Journal of Heat and Mass Transfer 261 (2026) 128581

Contents lists available at ScienceDirect

International Journal of Heat and Mass Transfer

journal homepage: www.elsevier.com/locate/ijhmt

Improved transient plane source measurements of layer–substrate structures via a semi-analytical temperature response model

Zijin Zeng [a,b,*], Christian Müller [a], Johan Gustavsson [c], Besira Mihiretie [b]

[a] *Department of Chemistry and Chemical Engineering, Chalmers University of Technology, Gothenburg 41296, Sweden*
[b] *Hot Disk AB, Sven Hultins gatan 9A, Gothenburg 41288, Sweden*
[c] *Thermetrol AB, Sven Hultins gatan 9A, Gothenburg 41288, Sweden*

ARTICLE INFO

Keywords:
Transient plane source method
Thin layer
Thermal conductivity
Thermal contact resistance
Finite element method

ABSTRACT

The Transient Plane Source (TPS) method is widely used to investigate the thermal properties of homogeneous bulk materials and has been further extended to layer–substrate structures. Conventional models on layer–substrate structures typically assume one-dimensional (1D) heat flux across the layer from the heating area into the backing substrate. This assumption imposes a series of constraints on the layer (thermal conductivity < 2 W $\mathrm{m^{-1}K^{-1}}$ and thickness < 600 μm) and on the heating area (radius > 11 mm), which greatly limits the scope of the current method. In this study, we present a new semi-analytical model with consideration of non-1D heat flux within the layer, along with an iterative algorithm which automatically selects time range for data analysis. This new model substantially relaxes these constraints, expanding the applicable layer thermal conductivity by an order of magnitude (up to 20 W $\mathrm{m^{-1}K^{-1}}$) and thickness by about three times (up to 2000 μm). Moreover, the model enables the use of a new TPS probe for layer-substrate structures, which has a radius of only 6.6 mm. Experiments are described to validate the new model, showing that inaccuracies primarily stem from the thermal contact resistance. Finite element simulations further indicate that a measurement accuracy better than 10 % can be achieved provided that thermal contact resistance is mitigated.

1. Introduction

Accurate characterization of material thermal properties, including thermal conductivity (λ) and thermal diffusivity (α), is essential for understanding and optimizing a broad range of engineering processes [1–3]. The Transient Plane Source (TPS) method is one of the most widely used characterization techniques, offering fast and non-destructive measurements [4,5]. Originally proposed in 1991, an international standard for the TPS method was introduced in 2008 [6].

A TPS measurement involves a flat probe — fabricated as a disk [4,5], rectangle [4] or other planar shape that is embedded between two identical solid or liquid samples. The most widely used design is the disk-shaped “Hot Disk” probe, which consists of a double-spiral metal foil sandwiched between thin insulating layers such as polyimide sheets [6]. The insulation layers provide electrical insulation and protection under different measurement conditions. The probe acts as both a heat source for the surrounding material and a thermometer to measure the resulting temperature response [6]. The thermal properties of bulk samples, including thermal conductivity and thermal diffusivity, can be simultaneously determined based on the recorded temperature response [4,6].

Upon heating by the probe, the temperature response (as a function of time t) of the sample surface in immediate contact with the probe ($\Delta T_{\mathrm{surf}}(t)$) is raised, typically by a few Kelvins. Based on the assumption that the spiral probe can be approximated by a number of concentric and equally spaced circular rings, the relationship between $\Delta T_{\mathrm{surf}}(t)$ and the thermal properties of the sample can be expressed as [6]:

$$\Delta T_{\mathrm{surf}}(t) = P_0\left(\pi^{\frac{3}{2}}R\lambda\right)^{-1} D(\tau) \text{ and } \tau = \left(\frac{t}{\theta}\right)^{\frac{1}{2}},\ \theta = \frac{R^2}{\alpha} \tag{1}$$

Where P_0 is the power output of the probe, R denotes the radius of the outermost ring of the probe, λ is the thermal conductivity of the sample, and α is the thermal diffusivity. $D(\tau)$ is the dimensionless shape function, defined as [6]:

---

* Corresponding author at: Chalmers University of Technology, Sweden.
E-mail address: zijin@chalmers.se (Z. Zeng).

https://doi.org/10.1016/j.ijheatmasstransfer.2026.128581
Received 31 October 2025; Received in revised form 9 February 2026; Accepted 19 February 2026
Available online 26 February 2026

Nomenclature

Symbols

P_0	power output of the probe
$\widehat{T}_{\mathrm{avg},t}$	the measured temperature response of the probe at time t
$\widehat{t}_{\alpha_l}$	t_{α_l} estimated by the empirical equation
$\mathscr{L}^{-1}$	inverse Laplace operator
ΔT_{pi}	additional temperature increase caused by polyimide sheets covering the probe
D_{o}	dimensionless shape function for an ideal circular heat source
I_0	first kind modified Bessel function of the zeroth order
I_1	first kind modified Bessel function of the first order
J_0	Bessel function of the first kind of order zero
J_1	Bessel function of the first kind of the first order
L_{pi}	thickness of the polyimide layer
R_l	radius of the sample layer
$R_{\mathrm{th},l}$	total thermal resistance between the probe and the substrate in a layer measurement
$R_{\mathrm{th},s}$	thermal resistance in case of a substrate measurement without a layer
R_{th}	thermal resistance between the probe and the background bulk material
S_{α_l}	sensitivity of T_{avg} to the thermal diffusivity of the sample layer
S_{α_s}	sensitivity of T_{avg} to the substrate thermal diffusivity
S_{λ_l}	sensitivity of T_{avg} to the thermal conductivity of the sample layer
S_{λ_s}	sensitivity of T_{avg} to the thermal conductivity of the substrate
S_x	sensitivity of T_{avg} to a specific parameter x
$T_{\mathrm{avg},t}$	The calculated temperature response of the probe at time t
n_G	size of the group G
q_i	$\sqrt{\beta^2 + p/\alpha_i}$
t_{α_l}	time at which the influence of the layer thermal diffusivity on ΔT_{avg} becomes minimal
t_{end}	ending time of the time window used for data analysis
t_{first}	first point of the measurement data
t_{start}	starting time of the window used for data analysis
λ_{pi}	thermal conductivity of the polyimide layer
$\mathscr{L}$	Laplace operator
t	time
ΔT_{add}	additional temperature difference
ΔT_{avg}	average temperature response of the probe
$\Delta T_{\mathrm{surf,o}}$	temperature response of the sample surface in immediate contact with the probe, in the case with an ideal circular heat source
ΔT_{surf}	temperature response of the sample surface in immediate contact with the probe
D	dimensionless shape function
G	group of t_{α_l} for different thicknesses, classified by material type
K	key term inside the inverse Laplace transform
L	thickness of the sample layer
R	radius of the outermost ring of the probe
m	number of concentric ring sources
p	Laplace variable
u	normalized radial coordinates
v	normalized radial coordinates
α	thermal diffusivity
β	Hankel variable
δ	a small perturbation in a specific parameter x
ε	relative error between the estimated value and reference value
λ	thermal conductivity
σ	integration variable related to dimensionless time
τ	dimensionless time
φ	power density of an ideal circular heat source

Abbreviation

1D	one dimensional
2D	two dimensional
FEM	Finite Element Method
GHP	Guarded Hot Plate
MGE	maximum group error
MSE	Mean Squared Error
PARDISO	Parallel Direct Sparse Solver
PMMA	poly(methyl methacrylate)
TIM	thermal interface material
TPS	Transient Plane Source
TWA	Temperature Wave Analysis

Subscripts

add	additional
avg	average
est	estimated
l	sample layer
o	ideal circular heat source
pi	polyimide
ref	reference
s	backing substrate
surf	surface
th	thermal

$$D(\tau) = [m(m+1)]^{-2} \int_0^{\tau} \sigma^{-2} \left[\sum_{n=1}^{m} n \times \sum_{k=1}^{m} k \exp\left(\frac{-(n^2+k^2)}{4m^2\sigma^2} \right) I_0\left(\frac{nk}{2m^2\sigma^2} \right) \right] \mathrm{d}\sigma \tag{2}$$

Where m denotes the number of concentric ring sources, σ is an integration variable related to dimensionless time, and I_0 is the first kind modified Bessel function of the zeroth order.

In most cases, the insulation layer and thermal contact resistance impede the heat conduction between the probe and the sample, leading to an additional temperature difference ($\Delta T_{\mathrm{add}}(t)$) between the probe and the sample surface in contact with the probe [6]. $\Delta T_{\mathrm{add}}(t)$ approaches a constant value within a short time after the measurement begins. Therefore, the average temperature response of the probe ($\Delta T_{\mathrm{avg}}(t)$) that is recorded by the instrument can be expressed as [6]:

$$\Delta T_{\mathrm{avg}}(t) = \Delta T_{\mathrm{surf}}(t) + \Delta T_{\mathrm{add}} \tag{3}$$

When utilizing a Hot Disk probe with a very small space between the concentric rings, $\Delta T_{\mathrm{surf}}(t)$ approaches the average temperature increase of an ideal circular heating source on a semi-infinite substrate ($\Delta T_{\mathrm{surf,o}}(t)$). In this case, the dimensionless shape function for $\Delta T_{\mathrm{surf,o}}(t)$ becomes [4,7]:

$$D_{\mathrm{o}}\ (\tau) = \int_0^{\tau} \mathrm{d}\sigma\sigma^{-2} \int_0^1 v\mathrm{d}v \int_0^1 u\mathrm{d}u \cdot \exp\left(-\frac{u^2+v^2}{4\sigma^2} \right) I_0\left(\frac{uv}{2\sigma^2} \right) \tag{4}$$

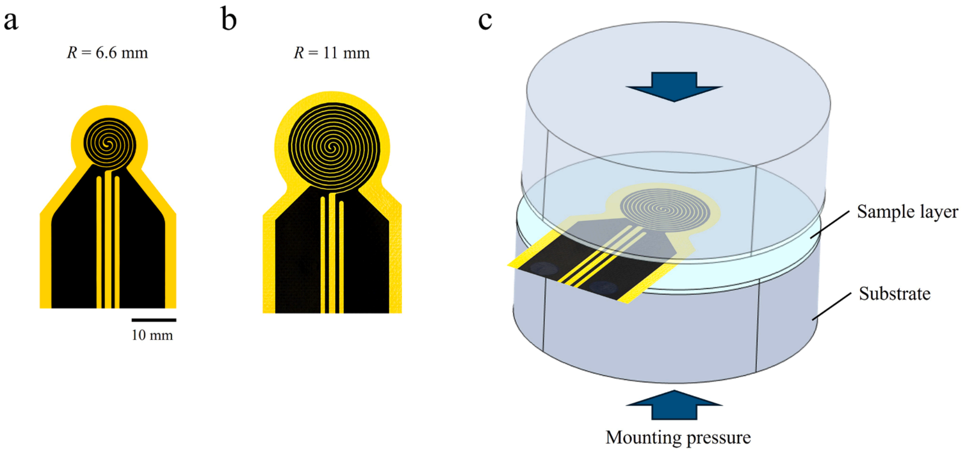

Fig. 1. (a-b) Probe profile featuring a nickel spiral foil sandwiched between polyimide sheets: (a) radius $R = 6.6$ mm, (b) radius $R = 11$ mm. (c) The vertically symmetrical configuration of a TPS measurement for layers. Two sample layers are positioned between the probe and the substrate.

Table 1
Conceptual comparison of TPS and its variants for layer-substrate structure.

Model	Conventional TPS [9]	TPS with empirical corrections [29]	CHS model [31]	This work
Assumptions	1D heat flux across the sample layer	1D heat flux across the sample layer, empirical correction for non-1D effects	1D heat flux across the sample layer	2D heat flux within the sample layer
Applicability	Limited layer thermal conductivity, thickness, and sensor radius	Limited layer thermal conductivity, thickness, and sensor radius	Supports asymmetric measurement configurations	Broader layer thickness and thermal conductivity, supports smaller sensors
Nature of approach	Analytical	Analytical with empirical corrections	Analytical reformulation	Analytical reformulation

where variable v and u represent normalized radial coordinates.

Laraqi also provided the explicit analytical expression of $\Delta T_{\mathrm{surf,o}}(t)$ [8]:

$$\Delta T_{\mathrm{surf,o}}(t) = \frac{\varphi R}{\lambda}\left(\frac{8}{3\pi}+2\sqrt{\frac{t^*}{\pi}}-2\sqrt{\frac{t^*}{\pi}}e^{-\frac{1}{2t^*}}\left[\left(1+\frac{2}{3t^*}\right)I_0\left(\frac{1}{2t^*}\right)\right.\right.$$
$$\left.\left.+\left(\frac{1}{3}+\frac{2}{3t^*}\right)I_1\left(\frac{1}{2t^*}\right)\right]\right) \tag{5}$$

where $t^* = \tau^2$, $\varphi = P_0/(\pi R^2)$ denotes the power density of an ideal circular heat source and I_1 is the first kind modified Bessel function of the first order.

Since the diameter of the probe is roughly two orders of magnitude larger than the thickness of polyimide insulation sheet, the heat flux between the probe and the bulk sample can be regarded as one dimensional (1D). ΔT_{add} can be used to estimate the thermal resistance (R_{th}) between the probe and the background bulk material (referred to as substrate) [6]:

$$R_{\mathrm{th}} = \frac{2\pi R^2 \Delta T_{\mathrm{add}}}{P_0} \tag{6}$$

If an additional thin layer is positioned between the probe and the substrate (Fig. 1 c), Eq. (6) still applies and can be used to obtain the corresponding thermal resistance. Consequently, the following equation allows to determine the thermal conductivity of the layer (λ_l) [6]:

$$R_{\mathrm{th},\ l} - R_{\mathrm{th},s} = \frac{L}{\lambda_l} \tag{7}$$

Here, L is the layer thickness, $R_{\mathrm{th},l}$ denotes the total thermal resistance between the probe and the substrate in a layer measurement when an extra layer is inserted, whereas $R_{\mathrm{th},s}$ is the thermal resistance in case of a substrate measurement without a layer.

This approach to utilizing the TPS method for thin layers was proposed in 1997 [9], and has since been adopted for characterizing polymer films [10–12], bio-based films [13,14], and polymeric composite films [15,16]. The thermal contact resistance encountered during a measurement can lead to an underestimation of the thermal conductivity [17,18]. This influence can be effectively mitigated by applying a thermal interface material (TIM), which is also used in conjunction with other contact-based methods such as the Guarded Hot Plate (GHP) method [19–21], the divided bar method [22], the 3w method with a reusable sensor [23], and the Temperature Wave Analysis (TWA) method [24]. In addition, thickness-dependent measurements can be employed to compensate for the influence of thermal contact resistance [10,25,26].

While the assumption of 1D heat flux greatly simplifies the equations used to calculate the thermal conductivity, it also imposes a principal limitation. The thermal conductivity and thickness of the sample layer must be strictly limited (< 2 Wm^{-1}K^{-1}, < 600 μm) to ensure that the heat flux across the layer remains strictly 1D. Otherwise, the influence of radial heat flux can lead to significant errors. This limitation means that a wide range of materials, such as alloys, ceramics, carbon-based materials, and composites with a relatively high thermal conductivity, cannot be characterized by the current layer measurement. Note that another TPS variant, the slab module [27,28], can be employed to characterize radial thermal conductivity of a slab, but satisfactory accuracy is obtained only for materials with a thermal conductivity over 10 W m^{-1} K^{-1} [28].

Theoretically, the assumption of 1D heat flux is also fulfilled if the sample and the probe are equal in size and perfectly aligned. However, ensuring these conditions requires precise shaping of the samples and careful alignment during assembly, which can significantly increase both the time and effort of the measurement process. Even small mismatches can introduce substantial errors, as evidenced by a study [18] showing that a 7 % difference in radius between the probe and the sample can result in errors of up to 15 %.

To the best of our knowledge, no previous study has addressed non-1D heat flux to extend TPS measurement capabilities in the context of

Table 2
Material properties.

Material	Thermal conductivity (W m^{-1} K^{-1})	Thermal diffusivity (mm^2 / s)	Density (kg /m^3)	Specific heat (J kg^{-1} K^{-1})
Stainless steel	13.5[a]	3.60[a]	8150[b]	460[a]
PMMA	0.21[a]	0.12[a]	1180[b]	1464[c]
Glass	1.34[a]	0.81[a]	2172[b]	766[c]
ZrO_2	3.15[a]	1.23[a]	6220[b]	412[c]
Al_2O_3	22.3[a]	7.26[a]	3775[b]	815[c]
Polyimide	0.12[d]	-	1090[d]	1420[d]
TIM	1.0 / 3.0[e]	-	2800[e]	-

[a] Measured by TPS measurements on bulk samples. The measurement accuracies are ±2 % for thermal conductivity and ±7 % for thermal diffusivity [6].

[b] Calculated from mass and volume.

[c] Measured by the Transient Plane Source Scanning method [45,47], with a measurement accuracy of approximately 5 %.

[d] Values from reference [48].

[e] Values from reference [49].

sample layers. Several investigations and model variants have been introduced but continue to adhere to the 1D heat flux assumption. Zhang et al. [29] systematically studied the influence of non-1D heat flux through a numerical simulation. An empirical function was proposed to compensate for non-1D heat flux, which was however only applicable to samples with a low thermal conductivity and limited thickness (Table 1). By approximating the layer as a lumped thermal resistance, Emanuel et al. [30,31] presented an analytical solution in integral form to describe the temperature fields generated by a circular heat source (CHS) in an asymmetric configuration (Table 1), i.e. with different layers and substrates on both sides of the heat source. The proposed CHS model was validated by comparing its results with those obtained from a reliable numerical model based on the finite element method (FEM). To decouple the effect of thermal contact resistance at the probe-sample interface, Landry et. al [18] proposed a new measurement configuration with an additional slab piece between the sample layer and the probe. A corresponding 1D model in the Laplace domain was developed and processed using numerical algorithms. Overall, these existing TPS-based approaches for layer–substrate structures rely on the 1D heat flux assumption, which enables the sample layer to be treated as a lumped thermal resistance and reduces computational complexity. This assumption, however, inherently restricts the applicability of TPS measurements to thin layers with low thermal conductivity. An empirical correction method has been proposed to partially compensate for non-1D heat flux effects. However, its validity remains limited and case-dependent, and it does not fundamentally remove the underlying 1D assumption (Table 1).

Accounting for multidimensional heat conduction within the multilayer structures facilitates a more comprehensive understanding of the heat conduction. Beck et al. [32–34] developed mathematical formulations to study the temperature field in multi-dimensional and multi-layer bodies. Gui et al. [35] used the transmission-line technique to study two-dimensional (2D) heat conduction in multilayer thin-film structures exposed to laser-induced surface-heating. Hui et al. [36,37] developed a 2D series solution to study the temperature distribution of a heat spreader on a semi-infinite heat sink. Milošević et al. [38] proposed a 2D analytical model for measuring the thermal diffusivity of two-layer slabs. Rassy et al. [39,40] proposed a three-dimensional semi-analytical model for a coating-substrate material in an unconventional laser flash measurement. This model enables the simultaneous identification of the direction-dependent thermal diffusivities of the coating. Cahill et al. [41] developed an iterative algorithm for calculating the frequency-domain temperature response of layered structures. This temperature is then converted into a transient temperature response to evaluate the accuracy of TPS-based measurements of thermal effusivity. Zheng et. al [42,43] proposed several analytical models to extend the capability of TPS measurements for bulk samples with low (~ 0.03 W m^{-1} K^{-1}) or relatively high thermal conductivity (> 30 W m^{-1} K^{-1}). These studies have provided valuable insights into multi-dimensional temperature responses during thermal property measurements, but these methods cannot be directly applied to the TPS technique for characterizing layer–substrate structures.

In this work, the objective is to extend the applicability of TPS measurements for layer–substrate structures beyond the limitations imposed by the conventional 1D heat flux assumption. To achieve this, we first develop a novel semi-analytical model that explicitly accounts for 2D heat flux within the sample layer by reformulating the governing heat conduction problem, thereby enabling accurate prediction of the temperature response for layers with higher thermal conductivity and larger thickness (Table 1). Second, a sensitivity analysis is conducted to identify appropriate analysis time windows for reliable determination of the layer thermal conductivity. Finally, based on these insights, an automated iterative fitting algorithm is developed to enable robust and efficient processing of TPS measurement data.

2. Measurement and mathematical models

2.1. Measurement setup

The TPS measurements of the layers were conducted using a TPS 2500 S Thermal Constants Analyzer from Hot Disk AB, Sweden. Two types of probes with a radius of 6.6 mm (Fig. 1 a) and 11 mm (Fig. 1 b) are utilized in the measurements. The sensing element (black) is made of a nickel spiral foil with four extending leads, two thin and two wide ones. The nickel spiral foils have a width of 870 μm and a thickness of 10 μm, with an inner spacing of 130 μm. The polyimide insulation sheets (yellow) have a thickness of 20 μm and ensure electrically insulation and protection. The substrates were stainless steel blocks with a thermal conductivity of 13.5 W m^{-1} K^{-1} (See Table 2 for material properties). The sample layer consists of poly(methyl methacrylate) (PMMA), zirconium dioxide (ZrO_2), stainless steel, or Alumina (Al_2O_3, 96 wt%) with thicknesses ranging from 500 μm to 2000 μm. To reduce thermal contact resistance, a high-thermal-conductivity, easily spreadable TIM is applied at the interface between the components (NT-H2 from Noctua, Austria). In addition, a controlled mounting force of 300 N was applied to the measurement assembly through a compression stand obtained from Hot Disk, Sweden. In the present study, the influence of mounting force is assumed to be minor when a readily spreadable TIM is used and the sample layer is mechanically stiff [26], such that variations in amounting force do not alter total thermal resistance between the probe and the substrate.

Based on the illustrated measurement setup (Fig. 1 c), both analytical and FEM models are developed to describe the heat transfer process. Analytical models are typically fast and capable of capturing the dominant heat transfer behavior, but they require more assumptions to approximate the actual experiment. The first common assumption in analytical models is that the probe can be regarded as an ideal circular boundary heat source, and the measurement setup can be assumed to be axisymmetric [18,30,42]. Accordingly, the analytical models are formulated in 2D cylindrical coordinates. The second common assumption is that the influence of thermal contact resistance is negligible, which is reasonable when TIMs are applied and the layer does not have an extremely high thermal conductivity. The validity of this assumption under the present experimental conditions is further evaluated and quantitatively discussed through finite-element simulations and experimental comparison in Section 4.2.

By contrast, FEM models are generally more robust, capable of investigating complex geometries. Although measurement data can be fitted with FEM models to estimate material properties [44,45], this approach is currently significantly more computationally demanding than the use of analytical solutions. As a result, FEM is primarily used to

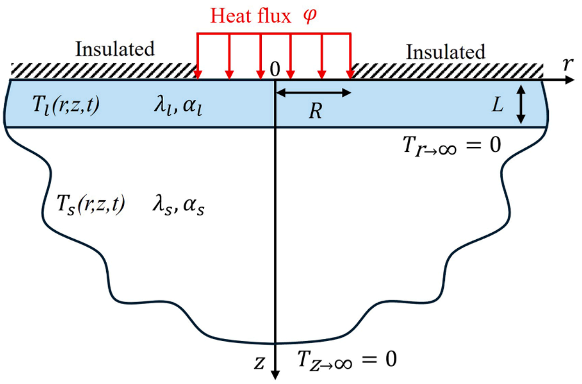

Fig. 2. Schematic of a semi-infinite substrate with a layer on top, subjected to uniform surface heating.

generate reference datasets to validate analytical models in this work [30,31,42,43].

In this study, four models are introduced and summarized as follows:

- **Layer 1D model**: An analytical model that assumes 1D heat flux across the layer (Section 2.2.2).
- **Layer 2D model**: A semi-analytical model that accounts for 2D heat flux across the layer (Section 2.2.3).
- **Simplified FEM model**: A FEM model based on the same physical configuration as the Layer 2D model, used to preliminarily assess the mathematical accuracy of the analytical models (Section 2.3.1).
- **Detailed FEM model**: A high-fidelity FEM model that closely represents the measurement setup, used to generate simulated measurement data for comprehensive evaluation of the analytical models (Section 2.3.2).

2.2. *Analytical models*

2.2.1. *Physical configuration and its solution*

The simplified physical configuration for analytical models is represented in cylindrical coordinates (Fig. 2). A semi-infinite substrate is in perfect thermal contact with a radially infinite overlying layer of thickness L. This layer-substrate assembly, initially at zero reference temperature, is suddenly subjected to heating across a circular area of radius R and a constant and uniform density φ. The remaining boundaries are assumed to be thermally insulated (adiabatic). The governing equation of heat diffusion in the solids is [46]:

$$\frac{\partial^2 T_i}{\partial r^2} + \frac{\partial T_i}{r\partial r} + \frac{\partial^2 T_i}{\partial z^2} = {\alpha_i}^{-1}\frac{\partial T_i}{\partial t} \tag{8}$$

where T represents the temperature response of the solids to the heating, α denotes thermal diffusivity, and $i = l$ or s corresponds to the layer and the substrate, respectively.

The boundary conditions are given by:

$$-\lambda_l \left.\frac{\partial T_l}{\partial z}\right|_{z=0} = \begin{cases} \varphi & (r \le R) \\ 0 & (r > R) \end{cases} \tag{9}$$

$$T_i(r, z, 0) = 0 \tag{10}$$

$$T_l(r\to\infty) = 0 \tag{11}$$

$$T_s(z\to\infty) = 0 \tag{12}$$

At the interface between the layer and the substrate where $z = L$ the following conditions apply:

$$T_l(z=L) = T_s(z=L) \tag{13}$$

$$-\lambda_l \left.\frac{\partial T_l}{\partial z}\right|_{z=L} = -\lambda_s \left.\frac{\partial T_s}{\partial z}\right|_{z=L} \tag{14}$$

The following Laplace and infinite Hankel transforms can be sequentially applied to Eqs. (8 - 9) and (12 - 14):

$$\overline{T}_i = \mathscr{L}\{T_i\} = \int_0^\infty T_i e^{-pt}\,\mathrm{d}t \tag{15}$$

$$\widetilde{\overline{T}}_i = \int_0^\infty rJ_0(\beta r)\overline{T}_i\,\mathrm{d}r \tag{16}$$

where $\mathscr{L}$ represents the Laplace operator, p is the Laplace variable, J_0 denotes the Bessel function of the first kind of order zero, and β is the Hankel variable.

The transformed version of the governing equation and boundary conditions become:

$$\frac{d^2\widetilde{\overline{T}}_i}{\mathrm{d}z^2} - \left[\beta^2 + p_i \,/\, \alpha\right] \widetilde{\overline{T}}_i = 0 \tag{17}$$

$$\widetilde{\overline{\varphi}} = \varphi\frac{aJ_1(\beta R)}{p\beta} \tag{18}$$

$$-\lambda_l \left.\frac{d\widetilde{\overline{T}}_l}{dz}\right|_{z=0} = \widetilde{\overline{\varphi}} \tag{19}$$

$$\left.\widetilde{\overline{T}}_s\right|_{z\to\infty} = 0 \tag{20}$$

where J_1 denotes the Bessel function of the first kind of the first order.

At the interface where $z = L$, the transformed equations are:

$$\widetilde{\overline{T}}_l(z=L) = \widetilde{\overline{T}}_s(z=L) \tag{21}$$

$$-\lambda_l \left.\frac{d\widetilde{\overline{T}}_l}{dz}\right|_{z=L} = -\lambda_s \left.\frac{d\widetilde{\overline{T}}_s}{dz}\right|_{z=L} \tag{22}$$

Combining Eqs. (17-22), the following expression can be derived for the temperature at the heating surface ($z = 0$),

$$\widetilde{\overline{T}}_l(r, 0, p) = \frac{\widetilde{\overline{\varphi}}}{\lambda_l q_l}\cdot\frac{\lambda_s q_s \tanh(Lq_l) + \lambda_l q_l}{\lambda_l q_l \tanh(Lq_l) + \lambda_s q_s} \tag{23}$$

where $q_i = \sqrt{\beta^2 + p/\alpha_i}$.

The following inverse Hankel and Laplace transforms can be applied to obtain the temperature in the Laplace domain:

$$\overline{T} = \int_0^\infty \beta J_0(\beta r)\widetilde{\overline{T}}\,d\beta \tag{24}$$

With this inverse transformation, Eq. (23) can be written as:

$$\overline{T_l}(r, 0, p) = \frac{\varphi R}{\lambda_l}\int_0^\infty \frac{J_0(\beta r)J_1(\beta R)}{q_l p}\cdot\frac{\lambda_s q_s \tanh(Lq_l) + \lambda_l q_l}{\lambda_l q_l \tanh(Lq_l) + \lambda_s q_s}\,d\beta \tag{25}$$

By integrating this expression over r from 0 to R, the expression for the area-average temperature of the heating region in the Laplace domain can be obtained:

$$\overline{\Delta T_{\mathrm{avg}}} = \frac{2\varphi}{\lambda_l}\int_0^\infty \frac{J_1^2(\beta R)}{q_l p\beta}\cdot\frac{\lambda_s q_s \tanh(Lq_l) + \lambda_l q_l}{\lambda_l q_l \tanh(Lq_l) + \lambda_s q_s}\,d\beta \tag{26}$$

The average temperature of the heating area can be written as:

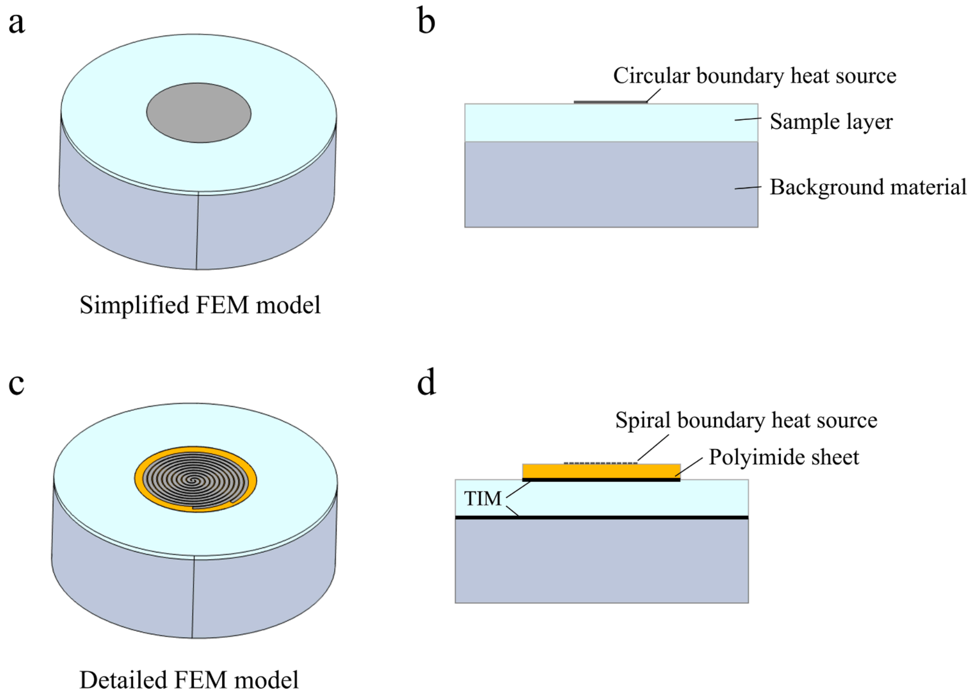

Fig. 3. Schematic of the (a) the Simplified FEM model and (c) the Detailed FEM model, along with their corresponding cross-sectional views in (b, d). Selected components in (b, d) are scaled to account for the wide range of dimensions, ensuring that all elements remain discernible.

$$\Delta T_{\text{avg}} = \frac{2\varphi}{\lambda_l}\int_0^{\infty}\frac{J_1^2(\beta R)}{\beta}\mathscr{L}^{-1}\left(\frac{1}{q_l p}\cdot\frac{\lambda_s q_s \tanh(Lq_l)+\lambda_l q_l}{\lambda_l q_l \tanh(Lq_l)+\lambda_s q_s}\right)d\beta \tag{27}$$

where $\mathscr{L}^{-1}$ denotes the inverse Laplace operator.

Several numerical algorithms are available that allow to calculate ΔT_{avg} directly based on Eq. (27). For example, the Talbot method can be employed to obtain the inverse Laplace transform and sequentially the composite trapezoidal rule can be used to calculate the integral with respect to β. However, this method is relatively time-consuming, hampering the application of Eq. (27) in data analysis. By introducing several reasonable assumptions, two simplified models, the 1D Layer Model and the 2D Layer Model, can be derived, each offering significantly reduced computation time at the cost of reduced accuracy in specific cases. The details of these models are described below.

2.2.2. Layer 1D model

When the layer has both a considerable small thickness ($L\rightarrow 0$) and a small thermal conductivity compared with the substrate ($\lambda_l \ll \lambda_s$), the heat flux across the layer can be regarded as 1D. In this case, $\tanh(Lq_l)\rightarrow Lq_l$ and $\lambda_l \tanh(Lq_l)\rightarrow 0$, which simplifies Eq. (27) to:

$$\Delta T_{\text{avg, 1D}} \approx \frac{\varphi L}{\lambda_l}+\frac{2\varphi}{\lambda_s}\int_0^{\infty}\frac{J_1^2(\beta R)}{\beta}\mathscr{L}^{-1}\left(\frac{1}{q_s p}\right)d\beta \tag{28}$$

The first term on the right side of Eq. (28) corresponds to an additional temperature increase caused by the layer, while the second term is the temperature increase of the bottom surface of the substrate in contact with the layer (Eq. (5)). Therefore, Eq. (28) can be written in explicit analytical form based on Laraqi's solution [8]:

$$\begin{aligned}\Delta T_{\text{avg, 1D}} \approx \frac{\varphi L}{\lambda_l}+\frac{\varphi R}{\lambda_s}\Bigg(\frac{8}{3\pi}+2\sqrt{\frac{t^*}{\pi}}-2\sqrt{\frac{t^*}{\pi}}e^{-\frac{1}{2t^*}}\Bigg[\left(1+\frac{2}{3t^*}\right)I_0\left(\frac{1}{2t^*}\right)\\ +\left(\frac{1}{3}+\frac{2}{3t^*}\right)I_1\left(\frac{1}{2t^*}\right)\Bigg]\Bigg)\end{aligned} \tag{29}$$

2.2.3. Layer 2D model

At a later stage of the measurement, the heat flux across the layer is assumed to achieve a quasi-steady state, where the contribution of α_l to ΔT_{avg} becomes negligible. During this stage, $\alpha_l = \alpha_s$ can be applied to simplify the term inside the inverse Laplace transform (K) in Eq. (27) (see Section S1 for full assumptions and derivation):

$$K = \frac{1}{pq_l}\cdot\frac{q_s \tanh(Lq_l)+c\cdot q_l}{c\cdot q_l \tanh(Lq_l)+q_s} \approx \frac{1}{pq_l}\cdot\frac{c(w^2+3)+3w}{(w^2+3)+3cw} \tag{30}$$

where $w = q_s L$ and $c = \lambda_l/\lambda_s$.

Upon taking the inverse Laplace transform of simplified K, the following equation can be written to predict ΔT_{avg}:

$$\Delta T_{\text{avg,2D}} = \frac{2\varphi}{\lambda_l}\int_0^{\infty}\frac{J_1^2(\beta R)}{\beta}\frac{(A+D)}{F}d\beta \tag{31}$$

where

$$A = c\left(\beta^4 L^4 - 3\beta^2 L^2 + 9\right)\cdot\operatorname{erf}\left(\beta\sqrt{\alpha_s t}\right)$$

$$D = 3\beta L\left(1 - c^2\right)\left(3+\beta^2 L^2\right)$$

$$F = 9\beta L + 3\beta^3 L^3\left(2 - 3c^2\right) + \beta^5 L^5$$

2.3. FEM models

In this study, two FEM models are developed. The first, a simplified FEM model, is used to generate reference data for validating the Layer 2D model and to highlight its improvement. The second one, referred to as the detailed FEM model, is employed to generate simulated temperature responses and investigate systematic measurement errors in the latter part of this paper.

These FEM models were developed using COMSOL Multiphysics (version 6.1) with the *Heat Transfer in Solids Module* and *Heat Transfer in Shell Module,* following a standard procedure reported in the literature [30,31,42,43]. The simulations were solved using the Parallel Direct

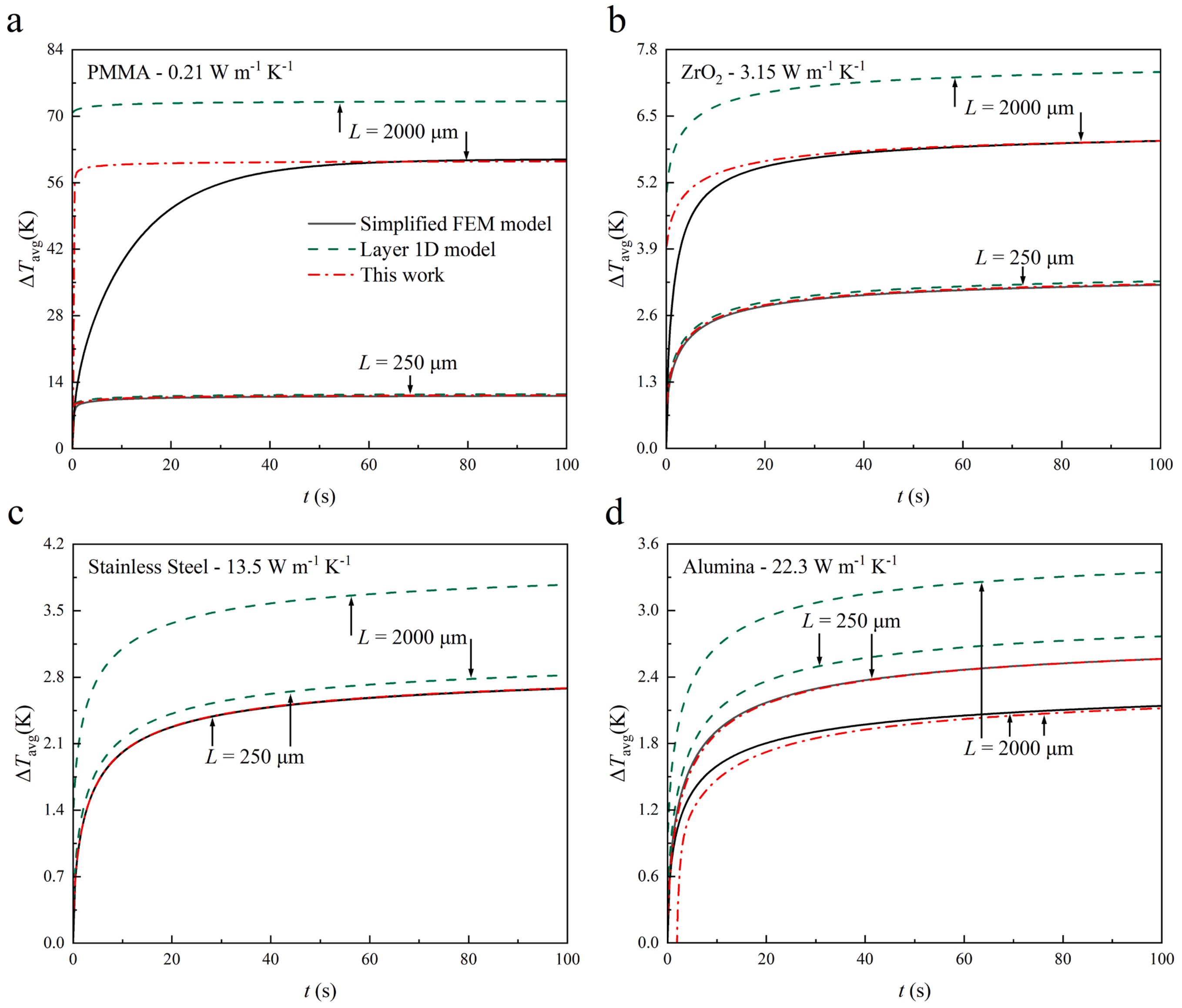

Fig. 4. Comparison of T_{avg} obtained using different models (Layer 1D model: green dashed line, Layer 2D model: red dash-dot line, Simplified FEM model: black solid line) for a heating area radius of 6 mm: (a) PMMA layer, (b) ZrO_2 layer, (c) stainless steel layer, and (d) alumina layer. The substrate in all cases is stainless steel, and the heating power is 1 W.

Sparse Solver (PARDISO). A mesh number of approximately 280000 and a solver relative tolerance of 10^{-7} were selected to ensure numerical stability, with corresponding independence analysis presented in Fig. S2.

2.3.1. Simplified FEM model

The geometry of the simplified FEM model (Fig. 3a) was developed according to the physical configuration in Fig. 2. The substrate is a stainless steel cylinder with a radius of 50 mm and a thickness of 38 mm (Fig. 3 b), which is sufficiently large to be considered a semi-infinite domain during the measurement. The sample layer is PMMA, ZrO_2, stainless steel or Al_2O_3 with thicknesses ranging from 250 μm to 2000 μm. On the top of the layer, there is a boundary heat source with a radius of 6 mm or 11 mm that provides uniform heat flux. All other boundaries are set as thermally insulated. Note that only half of the experimental setup was simulated owing to vertical symmetry in the heat conduction domain (See Table 2 for material properties used in the FEM simulations). Thermal contact resistance is not considered in this model.

2.3.2. Detailed FEM model

The detailed FEM model generates simulated measurement data to comprehensively evaluate the application of analytical models in data analysis. This model includes more details of the measurement setup compared with the simplified model. Specifically, a boundary heat source with a double spiral pattern is utilized to represent the actual heating element (Fig. 3 c). The influence of the four leads and heat capacity of the spiral is assumed to be negligible, which is reasonable provided that the samples do not have an extremely low thermal conductivity [42]. In addition, TIM are introduced to align with the experimental conditions.

3. Model verification and parameter estimation

3.1. Model comparison

To evaluate the accuracy of the analytical models, the values of T_{avg} calculated from the Layer 1D model and Layer 2D model are compared with those from a reference model — the Simplified FEM model (Fig. 4).

The conventional Layer 1D model agrees well with the FEM results in

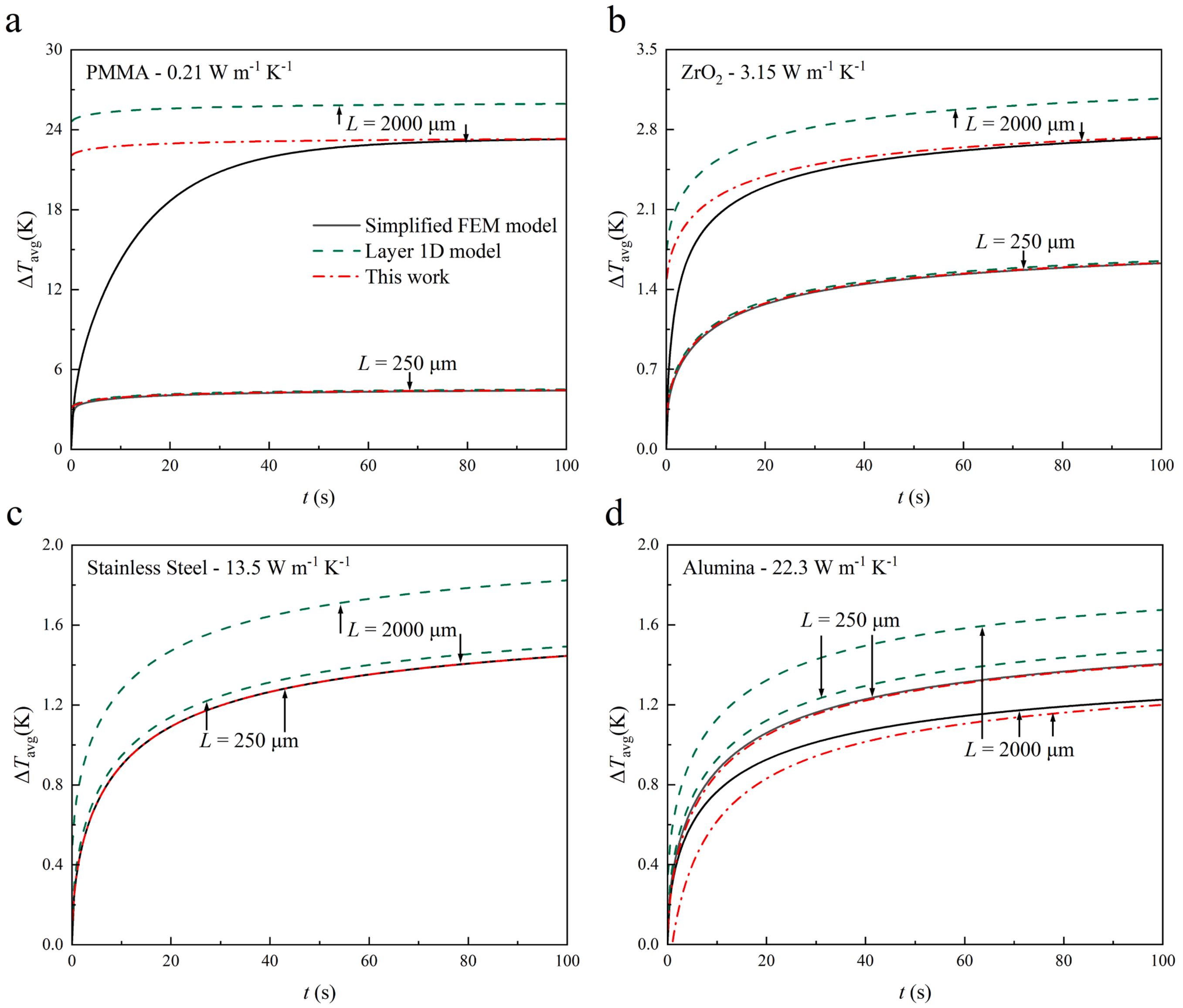

Fig. 5. Comparison of T_{avg} obtained using different models (Layer 1D model: green dashed line, Layer 2D model: red dash-dot line, Simplified FEM model: black solid line) for a heating area radius of 11 mm: (a) PMMA layer, (b) ZrO_2 layer, (c) stainless steel layer, and (d) alumina layer. The substrate in all cases is stainless steel, and the heating power is 1 W.

some cases — specifically, when the layer has both a low thermal conductivity and a small thickness (Fig. 4 a, bottom group). However, differences arise with higher thermal conductivity or layer thickness (Fig. 4 a-d). By contrast, the Layer 2D model agrees with the FEM model in the later stage, across a broad range of thermal conductivities (up to 20 W m^{-1} K^{-1}) and thicknesses (up to 2000 μm). Notably, the agreement is maintained when the thermal conductivity of the layer exceeds that of the substrate (Fig. 4 d).

In general, there is a time delay (denoted as t_{α_l} and discussed in Section 3.3) during which the Layer 2D model exhibits noticeable difference relative to the FEM results, after which close agreement is achieved. Beyond this delay, the point-wise maximum difference between the Layer 2D model and the reference results is approximately 0.4 %, except for the thickest alumina case, where the difference increases to approximately 1 %.

Theoretically, this time delay results from the simplification of heat diffusion within the layer in the equation, namely assuming $\alpha_l = \alpha_s$ (full assumptions available in Section S1). Therefore, this delay is linked to both the thickness and thermal diffusivity of the layer. It increases with increasing layer thickness and with a larger mismatch in thermal diffusivity between the layer and the backing substrate. For instance, in the case of PMMA, the delay increases from approximately 2 s to 60 s as the thickness increases from 250 μm to 2000 μm (Fig. 4 a). In the case of ZrO_2, which has a higher thermal diffusivity than PMMA, the delay becomes slightly smaller (Fig. 4 b). Estimating this delay is essential for applying this model and will be detailed in the following sections.

When layer and substrate share the same properties (Fig. 4 c, stainless steel layer on a stainless steel substrate), all scenarios with different thicknesses converge to the case of a semi-infinite substrate heated by a circular heat source. Therefore, the T_{avg} values remain identical across different layer thicknesses in both the simplified FEM model and Layer 2D model. The Layer 2D model closely aligns with the FEM throughout the whole period without any delay, as the assumption of $\alpha_l = \alpha_s$ is always fulfilled in these cases.

When the heating area has a larger radius (Fig. 5 a-d), the difference between the Layer 1D model and the FEM results is slightly reduced compared with the previous cases with a small heating area. Despite this reduction, the difference remains significant in most cases. The reduction is attributed to a higher ratio between the probe radius and the layer

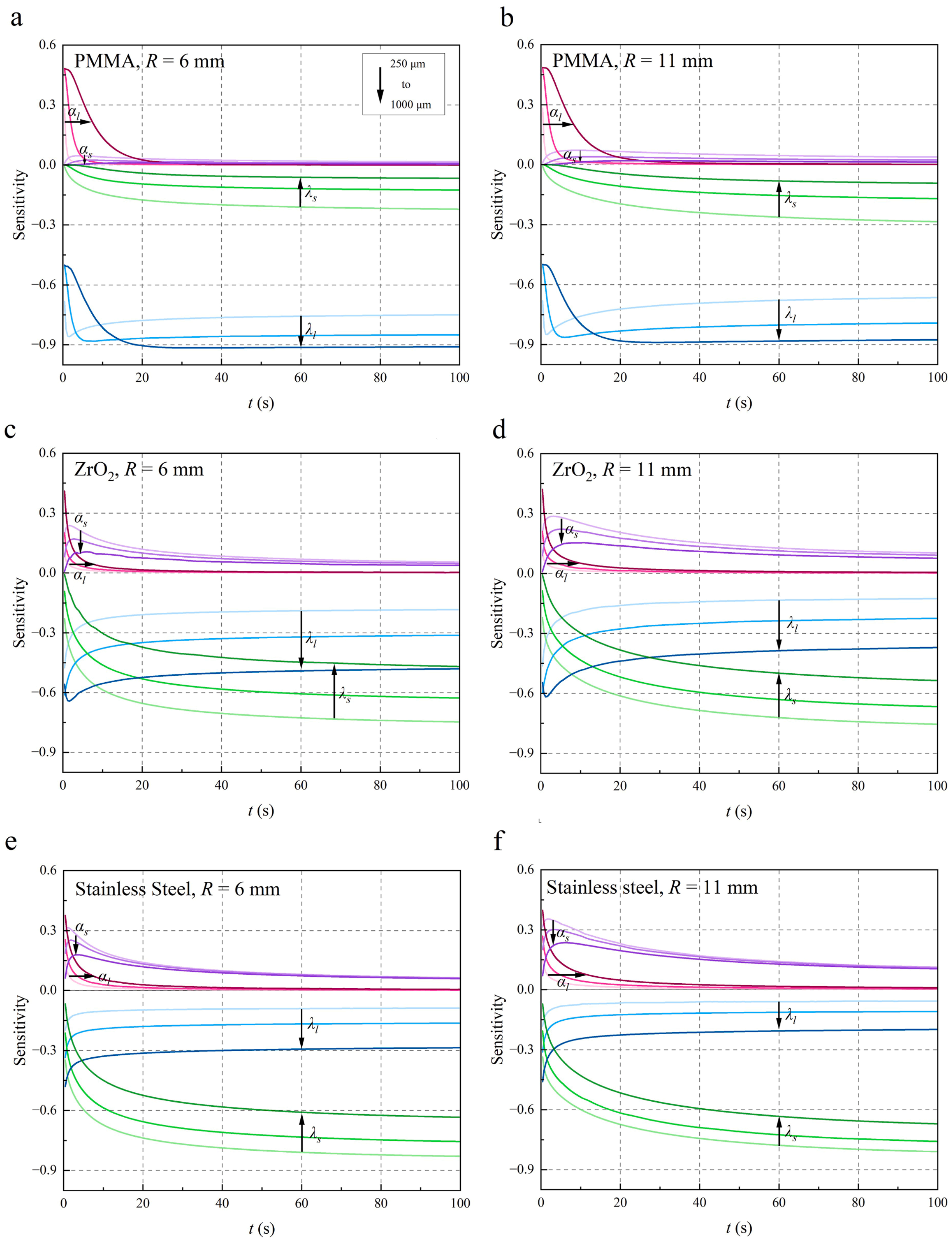

Fig. 6. Exemplary sensitivity of T_{avg} to different material properties at different layer thicknesses: (a-b) PMMA layer, (b-c) ZrO$_2$ layer, (e-f) stainless steel layer. The radius of heat source in (a), (c), and (e) is 6 mm, and 11 mm in (b), (d), and (f). In all cases, the substrate is stainless steel. The black arrow indicates the direction of increasing layer thickness.

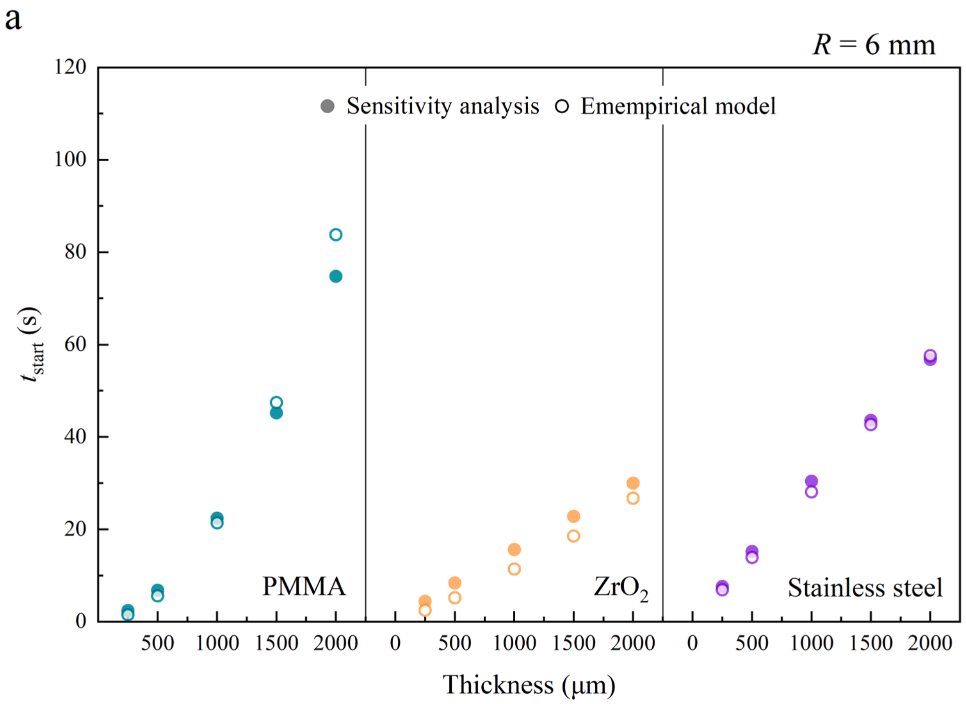

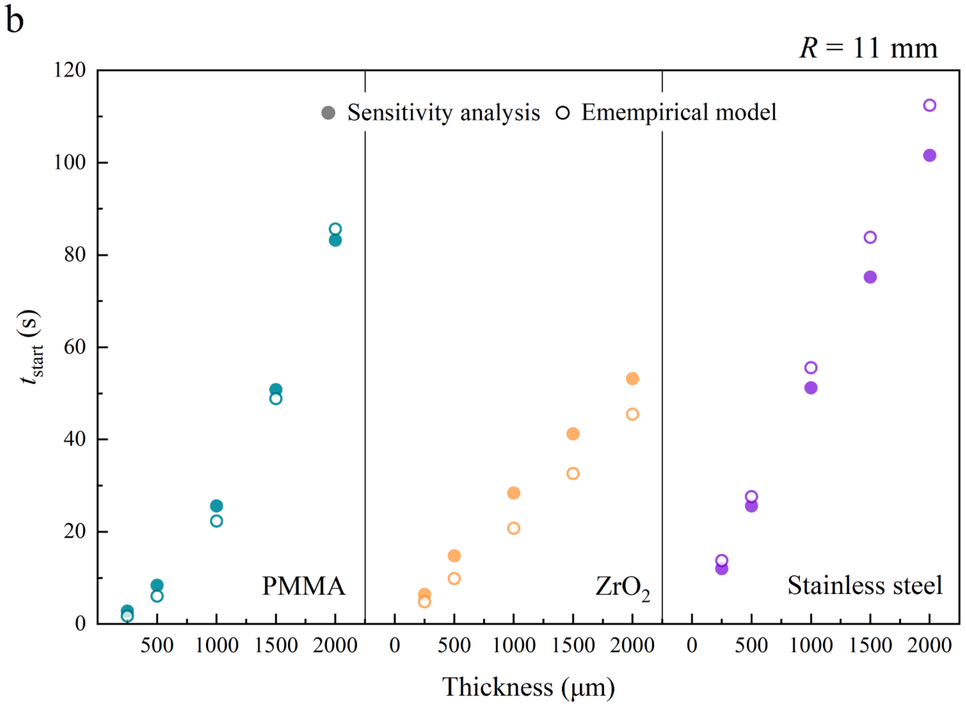

Fig. 7. Comparison of the estimated t_{start} obtained from sensitivity analysis (solid symbols) and the empirical model (empty symbols).

thickness, bringing the situation closer to the 1D heat flux assumption. However, even an 80 % increase in heating radius (from 6 to 11 mm) yields only marginal improvement, indicating that enlarging the heating area is not an effective strategy for improving the performance of the Layer 1D model.

On the other hand, the Layer 2D model still exhibits significantly better agreement with the FEM results after the time delay. In most cases, the maximum point-wise relative difference between the Layer 2D model and the reference results is approximately 0.4 %, similar to that obtained with a 6 mm heating area. For the thickest alumina layer, the maximum point-wise relative difference increases to about 2 %, which is slightly larger than that observed with a 6 mm heating area. Additionally, a slightly longer time is required for the Layer 2D model to achieve a good level of agreement with FEM results. For example, approximately 70 s are needed in the case of a 2000 μm thick ZrO$_2$ layer (Fig. 5 b), compared with 40 s when the heating area is smaller (Fig. 4 b). A longer time delay is undesirable, as it reduces the portion of the recorded data that can be used for data analysis when determining the thermal conductivity of the sample layer.

3.2. Sensitivity analysis

Based on the simplified FEM model, a sensitivity analysis is conducted to gain deeper insight into the interactions among parameters in

Table 3
Values of coefficients A, B and C used for predicting t_{α_l} with different heating radii.

Heating radius	A	B	C
6 mm	2.186	4.325	1.056
11 mm	2.483	5.889	1.140

the measurement, thereby guiding the design of the measurement scheme [43,50].

The sensitivity of T_{avg} to a specific parameter x is defined as:

$$S_x(t) = \frac{\partial \ln\left(T_{\text{avg}}(t)\right)}{\partial \ln(x)} \approx \frac{x\delta\left(T_{\text{avg}}(t)\right)}{T_{\text{avg}}(t)\ \delta(x)} \tag{32}$$

where δ presents a small perturbation. A large magnitude of $S_x(t)$ indicates that parameter x has a large influence on $T_{\text{avg}}(t)$. A positive $S_x(t)$ implies that $T_{\text{avg}}(t)$ increases as parameter x increases, and vice versa. Here, the data used for calculating $S_x(t)$ were obtained by a parameter sweep study in the FEM model with $\delta x = 0.02\ x$.

In all cases, the sensitivity to the layer thermal diffusivity (S_{α_l}) is initially high but quickly decreases to a minimal positive value over time (Fig. 6 a-f). The small value of S_{α_l} reflects the validity of the simplification of heat diffusion within the layer in the Layer 2D model, assuming $\alpha_l = \alpha_s$. For thinner layers, the magnitude of S_{α_l} decays more rapidly to a small value, explaining the shorter time delay they required to achieve agreement with the FEM results (Fig. 6 a–f). When the heating area is larger (Fig. 6 d-f), S_{α_l} is slightly higher and requires a longer time to decrease to a low value. This observation is in line with the results shown in Fig. 5, which shows a longer time is needed to achieve good agreement with the FEM model when a larger probe is used.

On the other hand, the sensitivity to layer thermal conductivity (S_{λ_l}) and substrate thermal conductivity (S_{λ_s}) are negative, and their magnitude increase with time (Fig. 6 a-f). In the case of PMMA (Fig. 6 a, d), the magnitude of S_{λ_l} is consistently greater than that of S_{λ_s} owing to its much lower thermal conductivity compared with the substrate. Increasing the layer thickness further increases the magnitude of S_{λ_l} and lowers that of S_{λ_s}. When both the layer and substrate are stainless steel (Fig. 6 c, f), S_{λ_l} has a higher magnitude in the very beginning (within 5 s) since the layer is in direct contact with the heating area. However, it is quickly surpassed by S_{λ_s} as time progresses. This case illustrates how the position influences the $S_x(t)$ when the layer and the substrate have the same properties. In general, the magnitude of S_{λ_l} is high, suggesting that λ_l can be reliably estimated.

3.3. *Estimation of time window*

To further utilize the Layer 2D model in analyzing the measurement data, it is essential to identify the appropriate time window $[t_{\text{start}}, t_{\text{end}}]$ during which this model can accurately describe the measurement results. Theoretically, a suitable t_{start} can be the time when the influence of the layer thermal diffusivity on ΔT_{avg} is very small, namely a minimal S_{α_l}. This time is denoted as t_{α_l} and can be extracted from sensitivity curves. Here, a value of t_{α_l} is assigned to the earliest time at which S_{α_l} falls below a threshold of 0.02 (Fig. 7 a, b, solid symbols). This sensitivity threshold is chosen to be sufficiently small so that the influence of α_l on the temperature response can be neglected, while its corresponding time point remains early enough to preserve a sufficiently long time window for further data analysis. To predict the extracted values of t_{α_l} and use it in the analysis of measurement data, an empirical equation is written with respect to the thickness and the thermal diffusivity of the layer:

$$\hat{t}_{\alpha_l} = \mathrm{A}\frac{L^2}{\alpha_l} + \mathrm{B}\frac{\alpha_l r^2}{\alpha_s}\left(\frac{L}{R}\right)^C \tag{33}$$

where A, B and C are constant to be determined for different heating radii. The first term is designed to represent the time that heat waves need to go through the layer in the vertical direction, while the second term is intended to be associated with the heat wave propagation in the radial direction. Constants A, B, and C are determined by an optimization process that minimizes the maximum group error (MGE) defined as:

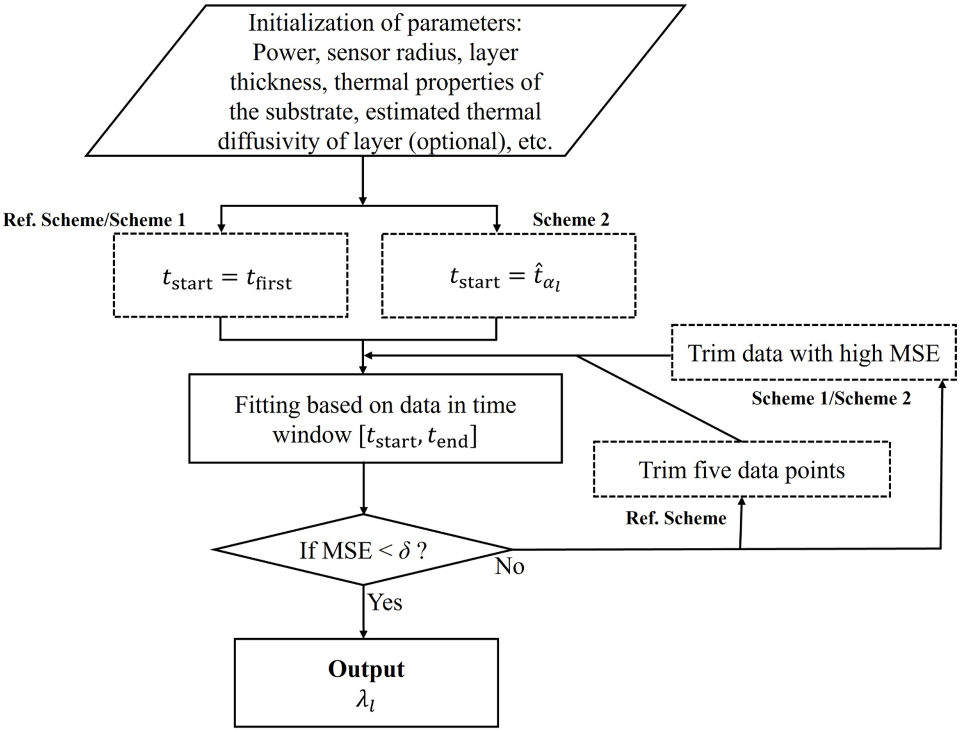

Fig. 8. Flow diagram of the iterative process used to determine the thermal conductivity of the layer.

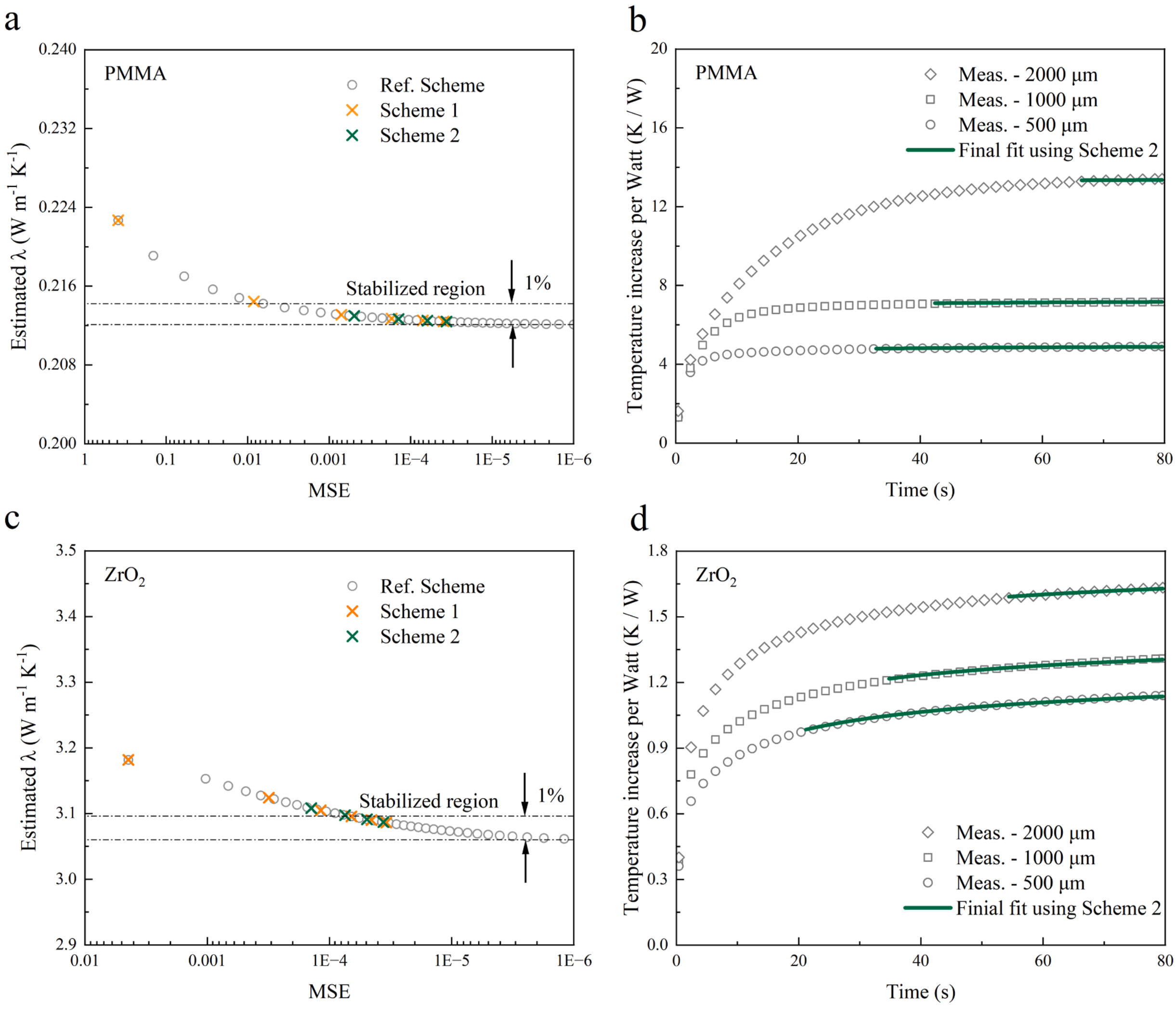

Fig. 9. Exemplary results from the fitting process. (a, c) Evolution of thermal conductivity values as a function of MSE using the reference scheme (grey), Scheme 1 (orange) and Scheme 2 (green), for a 500 µm-thick (a) glass and (c) ZrO_2 layer. (b, d) comparison between experimental T_{avg} data and the fitted data for (b) a glass layer and (d) a ZrO_2 layer.

$$\mathrm{MGE} = \max_G \left(\frac{1}{n_G} \sum_{j \in G} \left(\widehat{t}_{\alpha_l,\, j} - t_{\alpha_l,\, j} \right)^2 \right) \tag{34}$$

where G represents a group of t_{α_l} for different thicknesses, classified by material type, n_G is the size of the group G, j indexes t_{α_l} within each group.

For different sample layers on a stainless steel substrate using a fixed sensor radius, the constants A, B and C were determined through optimization (Table 3). The values of $\widehat{t}_{\alpha_l}$ predicted by Eq. (33) (empty symbols, Fig. 7 a, b) show alignment with that from sensitivity analysis, with a difference of less than 10 s. This level of agreement suggests that the empirical correlation provides a reasonable and consistent estimate within the investigated layer–substrate configurations.

3.4. Procedure of parameter estimation

In this section, several procedures are developed to apply the Layer 2D model for determining the thermal conductivity of layers using measurement data extracted from the Hot Disk software (Fig. 8). Overall, these procedures start with the initialization of parameters including heating power, probe radius, layer thickness, thermal properties of the substrate, etc. Afterwards, a fitting process is carried out over a specify time window $[t_{\mathrm{start}}, t_{\mathrm{end}}]$, using the Mean Squared Error (MSE) as the objective function:

$$\mathrm{MSE} = \frac{1}{n} \sum_{t=t_{\mathrm{start}}}^{t=t_{\mathrm{end}}} \left(T_{\mathrm{avg},t}(\lambda_l) - \widehat{T}_{\mathrm{avg},t} \right)^2 \tag{35}$$

where n is the number of data points in the time window, and $\widehat{T}_{\mathrm{avg},t}$ is the temperature response of the probe in the measurement. $T_{\mathrm{avg},t}(\lambda_l)$ is the temperature response of the probe calculated using the Layer 2D model, defined as:

$$\Delta T_{\mathrm{avg,2D}} = \Delta T_{\mathrm{pi}} + \frac{2\varphi}{\lambda_l} \int_0^\infty \frac{J_1^2(\beta R)}{\beta} \frac{(A+D)}{F} \, d\beta \tag{36}$$

where ΔT_{pi} is the additional temperature increase caused by polyimide sheets covering the probe. Owing to low thermal conductivity and small thickness of the polyimide sheets, ΔT_{pi} can be approximated as $\frac{\varphi L_{\mathrm{pi}}}{\lambda_{\mathrm{pi}}}$, where L_{pi} and λ_{pi} denote the thickness and the thermal conductivity of the polyimide sheets, respectively. The value of λ_{pi}, λ_s, and α_s used in Eq. (34) can be determined in a TPS measurement performed with the probe directly sandwiched between two substrates.

Three schemes are proposed to select and adjust the time window in

Table 4
The determined thermal conductivity of layers obtained from experimental data using the Layer 2D model. Each value represents the average of three repeated measurements, with the associated uncertainty given as the maximum difference among them. The maximum relative error ε with respect to reference values is below 7 % in all cases except alumina, for which the deviation reaches 34 % in the thinnest cases due to thermal contact resistance.

	Layer thickness (μm)	Thermal conductivity ($\mathrm{Wm^{-1}K^{-1}}$)				
		PMMA	Glass	ZrO_2	Stainless steel	Alumina
Probe A (R = 6.6 mm)	500	0.198 ± 0.001	1.35 ± 0.01	3.17 ± 0.18	13.8 ± 0.4	14.7 ± 0.1
	1000	0.196 ± 0.001	1.37 ± 0.02	3.15 ± 0.03	13.4 ± 0.3	22.4 ± 0.8
	2000	0.207 ± 0.001	1.33 ± 0.01	3.14 ± 0.01	13.9 ± 0.4	23.8 ± 0.2
Probe B (R = 11 mm)	500	0.206 ± 0.001	1.38 ± 0.03	3.11 ± 0.06	12.7 ± 0.6	18.4 ± 0.7
	1000	0.209 ± 0.011	1.42 ± 0.01	3.13 ± 0.06	13.9 ± 0.1	19.8 ± 0.6
	2000	0.212 ± 0.002	1.39 ± 0.06	3.22 ± 0.02	13.4 ± 0.3	22.6 ± 1.0

the fitting process: a reference scheme, Scheme 1, and Scheme 2. The reference scheme starts with all data points recorded in the measurement $[t_{\mathrm{first}}, t_{\mathrm{last}}]$ and iteratively adjusts the time window by trimming the first five data points at each step. Here, t_{first} and t_{last} represent the first and the last data point of the recorded data, respectively. The reference scheme is intended to provide baseline information about the relationship between time window, determined thermal conductivity, and MSE.

Similar to the reference scheme, Scheme 1 starts with time window $[t_{\mathrm{first}}, t_{\mathrm{last}}]$ but subsequently trims the segment with large square error, $\left(T_{\mathrm{avg},t}(\lambda_l) - \widehat{T}_{\mathrm{avg},t}\right)^2$. This trimming tactic aims to speed up the iterative process. Scheme 2, in turn, begins with the time window $[\widehat{t}_{\alpha_l}, t_{\mathrm{last}}]$ and likewise trims it by excluding the segment with the largest squared error. Here, $\widehat{t}_{\alpha_l}$ is estimated from an empirical equation using an approximate value of the layer thermal diffusivity (Eq. (33)). Overall, Scheme 1 is more general and can be utilized for random samples with unknown properties, while Scheme 2 can be employed when a rough value of thermal diffusivity is available, thereby further accelerating the iteration process.

Once the MSE falls below a predefined threshold (δ), the value of λ_l becomes the output value. Otherwise, the current time window is adjusted and used for another round of data fitting. After the fitting process, the relative error (ε) is used to evaluate the accuracy of the output thermal conductivity:

$$\varepsilon = \left(1 - \frac{\lambda_{l,\mathrm{est}}}{\lambda_{l,\mathrm{ref}}}\right) \cdot 100\ \% \tag{37}$$

where $\lambda_{l,\mathrm{est}}$ represents the λ_l estimated via the fitting process, while $\lambda_{l,\mathrm{ref}}$ represent the reference λ_l of the sample layer (Table 2). A positive value of ε corresponds to an overestimation of thermal conductivity, and vice versa.

4. Model application

4.1. Measurement results

The fitting results from the reference scheme are first analyzed. Even though a poor initial time-window (i.e., the full measurement window) is used, the iteration converges stably, demonstrating the robustness of the scheme. As the iteration progresses (Fig. 9 a, c), MSE decreases and the determined thermal conductivity tends toward a specific value. In particular, the variation of the determined thermal conductivity remains within 1 % once MSE falls below approximately 10^{-4} in cases of both glass and ZrO_2. Although trimming the time window by a small, fixed number of data points continuously lowers the MSE and eventually yields a precise thermal conductivity, this method requires more iteration steps and thus a longer execution time. Using a larger fixed step, e.g., 10 s or 20 s, can shorten the iterations but may cause overshooting and loss of accuracy.

In contrast to the reference scheme, Scheme 1 requires considerably fewer iteration steps to achieve the same MSE (orange symbols, Fig. 9 a, c). In case of glass and ZrO_2, only around five steps are required to achieve a minimal MSE of 10^{-4}, demonstrating a threefold improvement in efficiency compared with the reference scheme. When this tactic of adjusting the time window is combined with $\widehat{t}_{\mathrm{start}}$ estimated from the empirical equation (Scheme 2, green symbols, Fig. 9 a, c), only around three steps are required for both glass and ZrO_2, showing a further 30 % improvement in efficiency relative to Scheme 1. Overall, these two schemes show good robustness and stable convergence (Fig. 9 a, c), which we attribute to well-defined direction of progressively excluding data with large MSE. Note that both schemes require a sufficiently long measurement time, e.g., 80 s in our measurements, to ensure convergence.

Owing to its superior computational efficiency, Scheme 2 is employed to process all measurement data for determining the thermal conductivity of the sample layer. The fitting results exhibit stable and gradual convergence across a wide range of layer thermal conductivities and thicknesses, further confirming the robustness of the scheme in practical applications. The resulting fits show good agreement with the experimental data within the fitting window (Fig. 9 b, d). Moreover, the thermal conductivities determined using the Layer 2D model agree with the reference values in most cases (except for alumina), with errors ε below 7 % (Table 4), thereby validating the accuracy of the Layer 2D model. The magnitude of ε increases with higher layer thermal conductivity or reduced thickness, most likely dominated by the influence of thermal contact resistance. For comparison, the thermal conductivity determined by using the Layer 1D model is summarized in Table S1. Only a few cases (PMMA and glass layers thinner than 1000 μm) exhibit an acceptable ε of less than 14 %, highlighting the limitation of the Layer 1D model.

To reveal the distribution of ε with respect to layer thickness and thermal conductivity, contour maps are plotted based on the experimental data in Table S1 (Layer 1D model) and Table 4 (Layer 2D model). In the cases of a 6.6 mm probe (Fig. 10 a), the Layer 1D model yields low ε ($<$ 10 %) for low thermal conductivity and thin layers, since the assumption of 1D heat flux across the layer remains valid in these cases. However, ε increases dramatically with increasing thickness or thermal conductivity, which we attribute to the violation of the 1D heat flux assumption. It should be noted that the effect of this violation overshadows that of thermal contact resistance, ultimately leading to an overestimation of the layer thermal conductivity. In the case of a 11 mm probe (Fig. 10 b), the region with low ε ($<$ 10 %) is larger than the previous case. This is likely due to the increased probe-to-layer thickness ratio, which causes the heat flux within the layer to more closely approximate the assumed 1D scenario. The green frame in Fig. 10 b indicates the original applicability of TPS method for characterizing layers. Note that the data for layers thinner than 500 μm were not experimentally measured but derived by extrapolation from the measurement data.

When utilizing the Layer 2D model, the region with low ε covers the vast majority of the plot (Fig. 10 c,d) in cases of both a 6.6 mm and a 11 mm probe. We attribute this significant improvement to the consideration of 2D heat flux in the Layer 2D model. For layers thicker than approximately 750 μm or with a thermal conductivity lower than about

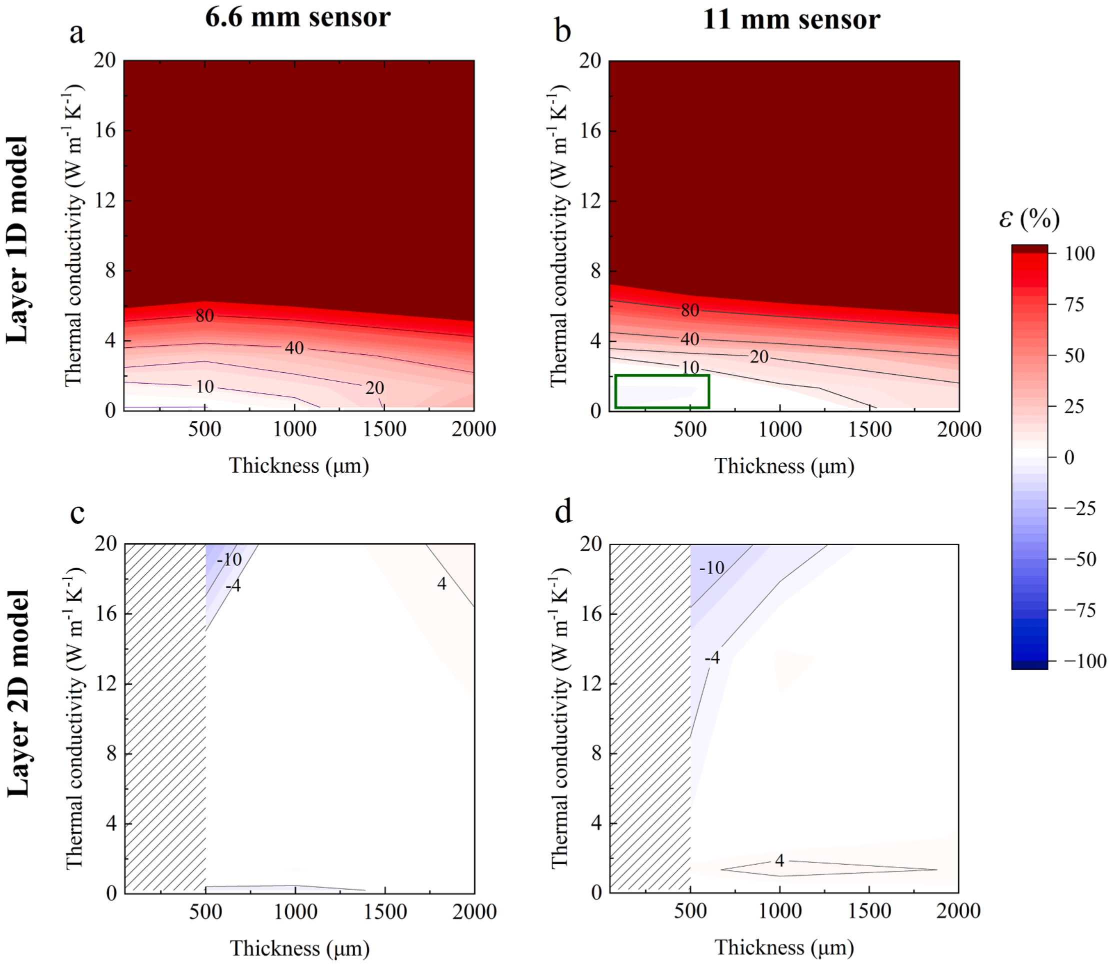

Fig. 10. Contour maps of error ε in layer thermal conductivity determined from measurement data using different probes and fitting models: (a) 6.6 mm probe, Layer 1D model, (b) 11 mm probe, Layer 1D model, (c) 6.6 mm probe, Layer 2D model, (d) 11 mm probe, Layer 2D model. Since the data for layers thinner than 500 μm was not experimentally obtained, the corresponding regions in (c,d) are shaded. In (a,b), due to pronounced overall gradient, the data of layers thinner than 500 μm was obtained by extrapolation based on the measurement data in Table S1.

8 W m^{-1} K^{-1}, ε is lower than 5 %. Only the upper left corner, corresponding to thermally thin layers, shows a magnitude of ε greater than 10 %, which we ascribe to the influence of thermal contact resistance.

4.2. Analysis of systematic errors

To further quantify systematic errors (e.g., those resulting from thermal contact resistance), the Layer 2D model is employed to determine the layer thermal conductivity from simulated measurement data generated by the detailed FEM model. The determined thermal conductivity is subsequently compared with the input value in the FEM model to calculate the relative error ε [30,31,42,43].

The simulated measurement data (Fig. 3 c, d) cover two thermal contact conditions between the probe, sample layer, and substrate: (i) good thermal contact, represented by a 5 μm-thick TIM with a thermal conductivity of 3 W m^{-1} K^{-1}, and (ii) inferior thermal contact, represented by a TIM of 1 W m^{-1} K^{-1}. By assuming 1D heat flux across the TIM layer, the thermal contact resistance caused by each TIM layer is estimated to be 2 mm^2 K W^{-1} in condition (i) and 5 mm^2 K W^{-1} in condition (ii).

When utilizing a TIM of 3 W m^{-1} K^{-1} (Fig. 11 a, b), ε is generally low ($<$ 10 %) for layers thicker than 250 μm in cases of both a 6.6 mm and 11 mm sensors. For thinner layers, thermal conductivity is slightly underestimated, consistent with the experimental observation. We attribute this underestimation to the thermal contact resistance between the components, which impedes thermal conduction and leads to a higher temperature response of the probe. For low thermal conductivity layers ($<$ 2 W m^{-1} K^{-1}), the magnitude of ε remains small even when the layer thickness is as low as 50 μm. Compared with the conventional Layer 1D model (green frame, Fig. 11 b), the measurement applicability is significantly extended, enabling accurate characterization ($\varepsilon <$ 10 %) of layers with higher thermal conductivities and greater thicknesses.

When the thermal contact resistance is higher (Fig. 11 c, d), the underestimation for thermally thin layers (left upper corner) becomes more pronounced, indicating that the thermal contact resistance is the primary limiting factor of the measurements. On the other hand, the results for thermally thick layers remain similar to those obtained with a TIM of 3 W m^{-1} K^{-1} TIM, indicating a negligible influence of the TIM thermal conductivity on these extracted values. In general, these results (Fig. 11 c, d) are closer to the measurement results observed in Fig. 10 c, d. Evidently, the influence of thermal contact resistance is not uniform but depends on the layer thickness and thermal conductivity. This influence is negligible for thick layers with low thermal conductivity, but becomes increasingly significant for thin layers with high thermal conductivity. Overall, although thermal contact resistance introduces minor systematic errors, they remain within an acceptable range for relatively thick layers and can be substantially reduced by improving thermal contact — for example, by using a TIM with higher thermal conductivity of 3 W m^{-1} K^{-1}.

The potential errors associated with finite radius of sample layer are

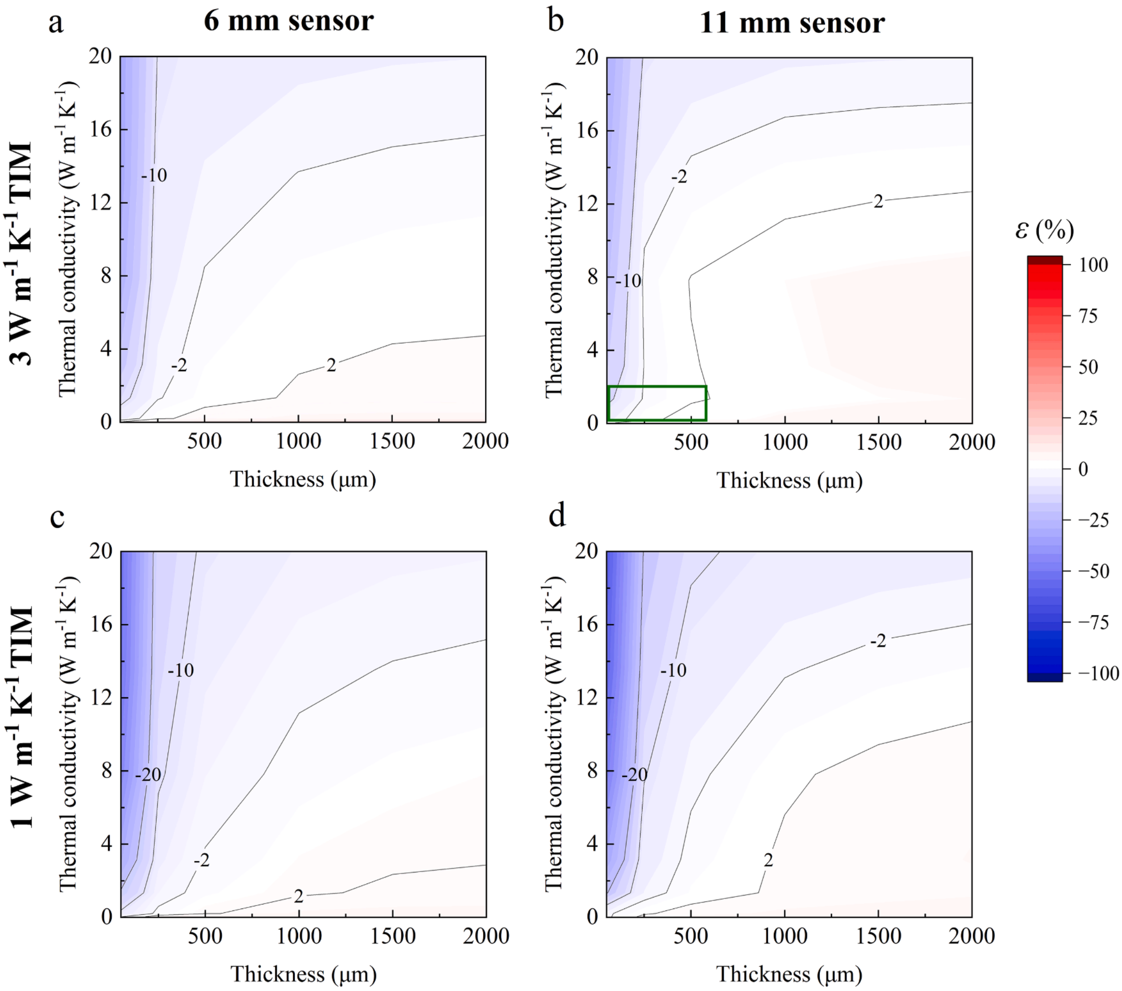

Fig. 11. Contour maps of relative error ε in the layer thermal conductivity determined using the Layer 2D model from simulated data under different conditions: (a) 6 mm probe, TIM thermal conductivity of 3 W m^{-1} K^{-1}, (b) 11 mm probe, TIM thermal conductivity of 3 W m^{-1} K^{-1}, (c) 6 mm probe, TIM thermal conductivity of 1 W m^{-1} K^{-1}, (c) 11 mm probe, TIM thermal conductivity of 1 W m^{-1} K^{-1}. The thickness of TIM for all cases is 5 μm.

also investigated (Fig. S3). If the radius of the sample layer is not sufficiently large — which may occur when the available sample material is limited, the assumption of a semi-infinite sample layer (Fig. 2) is no longer valid, leading to systematic errors. When the sample layer radius exceeds a threshold of 22 mm for a sensor radius of 6 mm, or 32 mm for a sensor radius of 11 mm (Fig. S3), T_{avg} becomes insensitive to further increases in radius. Under these conditions, the semi-infinite sample layer assumption is valid, and the corresponding systematic error in extracted thermal conductivity due to the finite radius of the sample layer is below 1 % for 11 mm sensor and 2 % for 6 mm sensor. Note that these radius thresholds are conservative. Smaller thresholds are expected to apply for sample layers with lower thermal conductivity or smaller thickness.

5. Conclusion

Conventional TPS measurements of layer-substrate structures rely on the assumption of 1D heat flux across the layer, which restricts their applicability to sample layers with low thermal conductivity (< 2 W m^{-1}K^{-1}), small thickness (< 600 μm), and relatively large probes (radius > 11 mm). In this work, we propose a semi-analytical model that accounts for non-1D heat flux across the layer. This new model is derived from the Laplace-Hankel transform and subsequently simplified for the regime where the heat flux within the layer reaches a quasi-steady state. Sensitivity analysis based on finite element simulations further validates this assumption and enables the development of an empirical equation to estimate the time range for data analysis. Overall, the new model demonstrates high accuracy for layers with a thermal conductivity up to 20 W m^{-1}K^{-1} (tenfold higher than before) and a thickness of up to 2000 μm (approximately threefold thicker). Moreover, this model enables the use of a new TPS probe for layer-substrate structures, featuring a radius of only 6.6 mm. Experimental validation confirms a substantially extended applicability range in both layer thermal conductivity and thickness. It should be noted that thermal contact resistance remains a limiting factor for thermally thin layers, such as an alumina layer with a thickness of 500 μm, even when a thermal interface material is applied. FEM simulations suggest that higher accuracy is attainable if the thermal contact resistance is further minimized, for example by using a thermal interface material with a higher thermal conductivity.

CRediT authorship contribution statement

Zijin Zeng: Writing – review & editing, Writing – original draft, Visualization, Validation, Methodology, Investigation, Formal analysis, Conceptualization. **Christian Müller:** Writing – review & editing, Supervision, Project administration, Funding acquisition. **Johan Gustavsson:** Writing – review & editing, Resources, Funding acquisition. **Besira Mihiretie:** Writing – review & editing, Supervision, Project administration, Funding acquisition.

Declaration of competing interest

The authors declare the following financial interests/personal relationships which may be considered as potential competing interests: Zijin Zeng reports a relationship with Hot Disk AB that includes: employment. Besira Mihiretie reports a relationship with Hot Disk AB that includes: employment. If there are other authors, they declare that they have no known competing financial interests or personal relationships that could have appeared to influence the work reported in this paper.

Acknowledgement

This project has received funding from the European Union's Horizon 2020 research and innovation program under the Marie Skłodowska-Curie grant agreement No 955837. The authors are grateful to Mr. Jesper Löfman for providing the high-resolution photographs of the Hot Disk probes.

Supplementary materials

Supplementary material associated with this article can be found, in the online version, at doi:10.1016/j.ijheatmasstransfer.2026.128581.

References

[1] D. Zhao, X. Qian, X. Gu, S.A. Jajja, R. Yang, Measurement techniques for thermal conductivity and interfacial thermal conductance of bulk and thin film materials, J. Electron. Packag. 138 (4) (2016) 040802.

[2] H. Wang, W. Chu, G. Chen, A brief review on measuring methods of thermal conductivity of organic and hybrid thermoelectric materials, Adv. Electron. Mater. 5 (11) (2019) 1900167.

[3] L. Kubičár, V. Boháč, P. Gaal, D. Apostolescu, Review of several dynamic methods of measuring thermophysical parameters, in: Proc. of 24th International Conference on Thermal Conductivity/12th International Thermal Expansion Symposium, Lancaster, PA, Technomic Publishing Co., 1999, pp. 135–149.

[4] S.E. Gustafsson, Transient plane source techniques for thermal conductivity and thermal diffusivity measurements of solid materials, Rev. Scient. Instrum. 62 (3) (1991) 797–804.

[5] S.E. Gustafsson, B.M. Mihiretie, M.K. Gustavsson, Measurement of thermal transport in solids with the hot disc method, Int. J. Thermophys. 45 (1) (2024) 1.

[6] ISO 22007-2:2022, Plastics — Determination of thermal conductivity and thermal diffusivty — Part 2: transient plane heat source (hot disc) method.

[7] Y. Jannot, Z. Acem, A quadrupolar complete model of the hot disc, Measur. Sci. Technol. 18 (5) (2007) 1229.

[8] N. Laraqi, Thermal impedance and transient temperature due to a spot of heat on a half-space, Int. J. Thermal Sci. 49 (3) (2010) 529–533.

[9] J. Gustavsson, M. Gustavsson, S. Gustavsson, On the Use of the Hot Disk Thermal Constants Analyser for Measuring the Thermal Conductivity of Thin Samples of Electrically Insulating Materials, Thermal Conductivity 24, Technomic Publishing Co., Lancaster, PA, 1997, pp. 116–122.

[10] M. Ahadi, M. Andisheh-Tadbir, M. Tam, M. Bahrami, An improved transient plane source method for measuring thermal conductivity of thin films: deconvoluting thermal contact resistance, Int. J. Heat. Mass Transf. 96 (2016) 371–380.

[11] M. Gustavsson, L. Hälldahl, Thermal conductivity measurements of thin insulating layers deposited on high-conducting sheets, Int. J. Thermophys. 27 (1) (2006) 195–208.

[12] Y. Zhang, T. Wang, X. Mei, M. Chen, L. Wu, Ordered porous polymer films for highly efficient passive daytime radiative cooling, ACS. Photonics. 10 (9) (2023) 3124–3132.

[13] W. Gan, Y. Wang, S. Xiao, R. Gao, Y. Shang, Y. Xie, J. Liu, J. Li, Magnetically driven 3D cellulose film for improved energy efficiency in solar evaporation, ACS. Appl. Mater. Interfaces. 13 (6) (2021) 7756–7765.

[14] X. Liu, H. Li, T. Zhang, H. Peng, K. Wang, Y. Dong, Y. Lu, K. Wang, X. Zhan, Y. Liu, Strong, tough, anisotropic, flexible, and transparent bamboo films, Ind. Crops. Prod. 207 (2024) 117757.

[15] Y. Guo, H. Qiu, K. Ruan, Y. Zhang, J. Gu, Hierarchically multifunctional polyimide composite films with strongly enhanced thermal conductivity, Nanomicro Lett. 14 (1) (2022) 26.

[16] T. Gu, Z. Zeng, S. Wu, D.-x. Sun, C.-s. Zhao, Y. Wang, Poly (L-lactic acid)/graphene composite films with asymmetric sandwich structure for thermal management and electromagnetic interference shielding, Chem. Eng. J. 466 (2023) 143190.

[17] H. Zhang, M.-J. Li, W.-Z. Fang, D. Dan, Z.-Y. Li, W.-Q. Tao, A numerical study on the theoretical accuracy of film thermal conductivity using transient plane source method, Appl. Therm. Eng. 72 (1) (2014) 62–69.

[18] D. Landry, R. Flores, R.B. Goodman, Estimating the thermal conductivity of thin films: A novel approach using the transient plane source method, ASME J. Heat Mass Transfer 146 (3) (2024) 031004.

[19] ASTM D5470-06, Standard test method for thermal transmission properties of thermally conductive electrical insulation materials, (2010).

[20] ASTM E1530-19, Standard test method for evaluating the resistance to thermal transmission of materials by the guarded heat flow meter technique, (2025).

[21] H.-P. Ebert, S. Vidi, Correct use of the guarded-hot-plate method for thermal conductivity measurements on solids, Int. J. Thermophys. 45 (2) (2024) 20.

[22] K. Horai, T. Shankland, Thermal conductivity of rocks and minerals, Method. Experim. Phys. 24 (1987) 271–302.

[23] D. Chalise, R. Tee, Y. Zeng, S. Kaur, H. Pokharna, R.S. Prasher, High throughput, spatially resolved thermal properties measurement using attachable and reusable 3 ω sensors, Rev. Scient. Instrum. 94 (9) (2023).

[24] A. Muscio, P.G. Bison, S. Marinetti, E. Grinzato, Thermal diffusivity measurement in slabs using harmonic and one-dimensional propagation of thermal waves, Int. J. Thermal Sci. 43 (5) (2004) 453–463.

[25] B. Feng, Y.-H. Zhang, J. Tu, L.-W. Fan, Z.-T. Yu, Determination on the thermal conductivity and thermal contact resistance of thin composite phase change films as a thermal interfacial material, Case Stud. Thermal Eng. 33 (2022) 101979.

[26] Z. Zeng, P. Sowinski, C. Müller, B. Mihiretie, Liquid interface for accurate intrinsic thermal conductivity measurements of polymer films using the transient plane source method, J. Therm. Sci. Eng. Appl. 17 (11) (2025) 111008.

[27] M. Gustavsson, E. Karawacki, S.E. Gustafsson, Thermal conductivity, thermal diffusivity, and specific heat of thin samples from transient measurements with hot disk sensors, Rev. Scient. Instrum. 65 (12) (1994) 3856–3859.

[28] Hot Disk Thermal Constants Analyser — Instruction Manual, Hot Disk AB, Sweden, 2023 downloaded in.

[29] H. Zhang, Y.-M. Li, W.-Q. Tao, Theoretical accuracy of anisotropic thermal conductivity determined by transient plane source method, Int. J. Heat. Mass Transf. 108 (2017) 1634–1644.

[30] M. Emanuel, M. Bhouri, S.L. Ackermann, D. Groulx, J. Maassen, Temperature fields generated by a circular heat source (CHS) in an infinite medium: analytical derivation and comparison to finite element modeling, Int. J. Heat. Mass Transf. 126 (2018) 1265–1274.

[31] M. Emanuel, M. Bhouri, J. Furlotte, D. Groulx, J. Maassen, Temperature fields generated by a circular heat source (CHS) in an infinite isotropic medium: treatment of contact resistances with application to thin films, Int. J. Heat. Mass Transf. 137 (2019) 677–689.

[32] A. Haji-Sheikh, J. Beck, D. Agonafer, Steady-state heat conduction in multi-layer bodies, Int. J. Heat. Mass Transf. 46 (13) (2003) 2363–2379.

[33] D.H. Yen, J.V. Beck, Green's functions and three-dimensional steady-state heat-conduction problems in a two-layered composite, J. Eng. Math. 49 (3) (2004) 305–319.

[34] L. Yan, A. Haji-Sheikh, J. Beck, Thermal characteristics of two-layered bodies with embedded thin-film heat source, J. Electron. Packag. 115 (3) (1993) 276–283.

[35] P. Hui, H. Tan, A transmission-line theory for heat conduction in multilayer thin films, IEEE Transac. Comp., Packag., Manufact. Technol. 17 (3) (2002) 426–434.

[36] P. Hui, H. Tan, Temperature distributions in a heat dissipation system using a cylindrical diamond heat spreader on a copper heat sink, J. Appl. Phys. 75 (2) (1994) 748–757.

[37] P. Hui, H.S. Tan, A rigorous series solution for a thermal dissipation system with a diamond heat spreader on an infinite slab heat sink, Jpn. J. Appl. Phys. 34 (9R) (1995) 5056.

[38] N.D. Milošević, M. Raynaud, Analytical solution of transient heat conduction in a two-layer anisotropic cylindrical slab excited superficially by a short laser pulse, Int. J. Heat. Mass Transf. 47 (8-9) (2004) 1627–1641.

[39] E. El Rassy, Y. Billaud, D. Saury, A direct method for the simultaneous characterization of thermal diffusivities of a bi-layer material consisting of a thin coating deposited on a substrate, Appl. Mathem. Modell. 91 (2021) 614–631.

[40] E. El Rassy, Y. Billaud, D. Saury, Unconventional flash technique for the identification of multilayer thermal diffusivity tensors, Int. J. Thermal Sci. 155 (2020) 106430.

[41] S. Yeon, D.G. Cahill, Analysis of heat flow in modified transient plane source (MTPS) measurements of the thermal effusivity and thermal conductivity of materials, Rev. Scientif. Instrum. 95 (3) (2024).

[42] Q. Zheng, S. Kaur, C. Dames, R.S. Prasher, Analysis and improvement of the hot disk transient plane source method for low thermal conductivity materials, Int. J. Heat. Mass Transf. 151 (2020) 119331.

[43] G. Jiaqi, S.B. Safiullah, L. Yang, Q. Ziyan, Q. Zheng, Improving the accuracy of transient plane source thermal conductivity measurements: novel analytical models, fitting approaches, and systematic sensitivity analysis, Int. J. Heat. Mass Transf. 247 (2025) 127110.

[44] V. Barragán, M. Izquierdo-Gil, J. Maroto, P. Antoranz, S. Muñoz, Estimation of the through-plane thermal conductivity of polymeric ion-exchange membranes using finite element technique, Int. J. Heat. Mass Transf. 176 (2021) 121469.

[45] Z. Zeng, C. Müller, B. Mihiretie, Extending the transient plane source scanning method for determining the specific heat capacity of low thermal conductivity materials through a numerical study, Thermochim. Acta 742 (2024) 179883.
[46] H.S. Carslaw, J.C. Jaeger, Conduction of Heat in Solids, Oxford Science Publications, New York, 2000.
[47] M. Gustavsson, N. Saxena, E. Karawacki, S. Gustafsson, Specific heat measurements with the hot disk thermal constants analyser, Thermal Conductivity 23, CRC Press, 1995, pp. 56–65.
[48] A.C. Lua, J. Su, Isothermal and non-isothermal pyrolysis kinetics of Kapton® polyimide, Polym. Degrad. Stab. 91 (1) (2006) 144–153.
[49] Thermal-Paste Comparison, Igor's lab. https://www.igorslab.de/en/thermal-paste-comparison/?ids=30, 2025.
[50] V. Bohac, M.K. Gustavsson, L. Kubicar, S.E. Gustafsson, Parameter estimations for measurements of thermal transport properties with the hot disk thermal constants analyzer, Rev. Scientif. Instrum. 71 (6) (2000) 2452–2455.